2018

Effect of chemical composition on microstructure, strength and wear resistance of wire deposited Ni-Cu alloys

Olexandra Marenych
University of Wollongong, Defence Materials Technology Centre, om753@uowmail.edu.au

Donghong Ding
University of Wollongong, Defence Materials Technology Centre, donghong@uow.edu.au

Zengxi Stephen Pan
University of Wollongong, Defence Materials Technology Centre, zengxi@uow.edu.au

Andrii Kostryzhev
University of Wollongong, andrii@uow.edu.au

Hui Jun Li
University of Wollongong, Defence Materials Technology Centre, huijun@uow.edu.au

See next page for additional authors

Effect of chemical composition on microstructure, strength and wear resistance of wire deposited Ni-Cu alloys

Abstract

Two Ni-Cu alloys (Monel K500 and FM 60) having various Mn, Fe, Al, Ti and C contents were deposited on a Monel K500 plate at three different speeds using wire arc additive manufacturing technique. Microstructure characterisation, in particular a detailed study of precipitates, was carried out using optical and scanning electron microscopy. Mechanical properties were assessed using hardness, tensile and wear testing. For similar deposition conditions, Monel K500 has exhibited smaller secondary dendrite arm spacing and higher number density of Ti-rich particles, although the Ti concentration in FM 60 was higher. Finer microstructure and Ti precipitation led to superior hardness, tensile and wear resistance of Monel K500 compared to FM 60. The variation in microstructure-properties relationship with alloy composition is discussed.

Disciplines

Engineering | Science and Technology Studies

Publication Details

Marenych, O. O., Ding, D., Pan, Z., Kostryzhev, A. G., Li, H. & van Duin, S. (2018). Effect of chemical composition on microstructure, strength and wear resistance of wire deposited Ni-Cu alloys. Additive Manufacturing, 24 30-36.

Authors

Olexandra Marenych, Donghong Ding, Zengxi Stephen Pan, Andrii Kostryzhev, Hui Jun Li, and Stephen van Duin

Additive Manufacturing 24 (2018) 30-36

Effect of chemical composition on microstructure, strength and wear resistance of wire deposited Ni-Cu alloys

O.O. Marenych[a, b], D. Ding[a, b], Z. Pan[a, b], A.G. Kostryzhev[a], H. Li[a, b], S. van Duin[a, b]

a. School of Mechanical, Materials, Mechatronics and Biomedical Engineering, University of Wollongong, Northfields Avenue, Wollongong, NSW 2500, Australia;
b. Defence Materials Technology Centre, Hawthorn, VIC 3122, Australia;
om753@uowmail.edu.au; donghong@uow.edu.au; zengxi@uow.edu.au; andrii@uow.edu.au; huijun@uow.edu.au; svanduin@uow.edu.au
Correspondence: zengxi@uow.edu.au; Tel.: +61-2-42215498

Abstract

Two Ni-Cu alloys (Monel K500 and FM60) having various Mn, Fe, Al, Ti and C contents were deposited on a Monel K500 plate at three different speeds using wire arc additive manufacturing technique. Microstructure characterisation, in particular a detailed study of precipitates, was carried out using optical and scanning electron microscopy. Mechanical properties were assessed using hardness, tensile and wear testing. For similar deposition conditions, Monel K500 has exhibited smaller secondary dendrite arm spacing and higher number density of Ti-rich particles, although the Ti concentration in FM60 was higher. Finer microstructure and Ti precipitation led to superior hardness, tensile and wear resistance of Monel K500 compared to FM60. The variation in microstructure-properties relationship with alloy composition is discussed.

Key words: Ni-Cu alloys; wire arc additive manufacturing; microstructure characterisation; mechanical properties; wear resistance.

Introduction

Nickel has good mechanical properties and excellent resistance to various corrosive environments. It is the “base” for the Ni-base alloys families, which are amongst the most important classes of engineering materials [1]. Ni-base alloys retain austenitic matrix from solidification to absolute zero that is why they can be used both at cryogenic temperatures and at temperatures approaching 1200 °C. They sustain high strength, ductility and toughness in this whole temperature range [2]. Ni-base alloys have a higher tolerance for alloying elements in solid solution than stainless steels and other iron-base alloys but maintain good metallurgical stability. These factors have resulted in development of Ni-base alloys with multiple alloying additions to provide wide variety of properties [3]. Major additions of copper (28-34%) provide solid solution strengthening [4] and improve the resistance of Ni to nonoxidizing acids [5, 3]. The Ni-Cu system has complete solid solubility, which allows production of single-phase alloys over the entire composition range [6]. The Ni-Cu system forms the basis for the Monel alloy family. Additions of Al and Ti help to produce a stronger version of the Ni-Cu alloy that would contain nano-size precipitates when properly heat-treated [7]. This alloy is known as Monel K500 and is widely used in marine industry to produce parts of heavy machinery, such as submarine propeller shafts, diesel engine piston rods, centrifugal pump shafts.

Despite its good mechanical and corrosion resistance properties, Monel K500 components may fail in operation. As this alloy is often used for manufacturing of machine parts with mating metal surfaces, wear is one of the key failure origins. Not only this directly affects equipment life, especially when operated in corrosion environment, but also it may endanger an entire mechanical system if a critical part is damaged [8]. Pitting corrosion, which is extremely localized corrosion leading to the creation of small holes on the surface, is another form of failure of Monel K500

components. Since Ni-base alloys are expensive, repair is often a more economic choice than replacement.

A promising alternative to traditional subtractive manufacturing is additive manufacturing or 3D printing. It can be applied not only for production of new functional components, but also for repair of old components. Based on the supply material (feedstock), additive manufacturing of metals can be divided into two major groups: one that deposits powder and another that deposits melted wire to build/repair a component. Powder-based principle has a number of downsides such as porosity, low deposition rates, component size limitation, high cost [9]. Wire-based deposition technologies, on the other hand, provide stronger adhesion of deposited layers due to full melting of wire, have higher production capacity, and often do not have component geometry restrictions. Moreover, wire-based additive manufacturing allows using of wire with a very complicated chemical composition which, when used for repair, gives an opportunity to deposit material with matching chemical composition to the damaged part.

Wire arc additive manufacturing (WAAM) has been closely investigated since the 1990s [10] to nowadays [11]. This technique combines an electric arc as heat source and a wire as feedstock and employs either gas metal arc welding (GMAW) [12], gas tungsten arc welding (GTAW) [13] or plasma arc welding (PAW) [14]. A consumable electrode is deposited layer by layer to manufacture a new component or repair an old component reducing material wastage and production/repair time [15]. This technique is advantageous due to its high deposition rate and low cost. A number of recent publications reported successful application of WAAM for fabricating of components made of Ti-base [16, 17], Fe-base [18, 19], Al-base [20], Cu-base [21] and Ni-base alloys (Ni-Cr) [22, 23]. However, the WAAM of Ni-Cu alloys has not been previously reported.

This study focuses on the WAAM of two Ni-Cu alloys, namely Monel K500 and FM60. Single-bead multi-layer wall structures as well as multi-bead single-layer plate structures have been successfully fabricated to investigate the microstructure and mechanical properties of wire arc additively manufactured Ni-Cu alloys. Particularly, the effect of chemical composition and heat input (wire deposition speed) on microstructure (in particular, particle precipitation), hardness, tensile strength and wear resistance was thoroughly investigated. If proved being successful, the WAAM of Ni-Cu alloys may provide an economic way of repairing the damaged parts instead of their entire replacement.

Materials and experimental techniques

Two welding consumables, commercially produced Monel K500 wire with diameter 1.0 mm and ERNiCu-7 (FM60) wire with diameter 1.2 mm were used in this study for comparison. A Monel K500 plate with dimensions 600x260x8 mm was used as the substrate. The chemical compositions of the materials are listed in Table 1.

Table 1. Chemical compositions of Monel K500 and FM60 used in the study (wt. %)

Alloy	Ni	Mn	Fe	Si	Al	Ti	C	S	P	Cu
Monel K500	68.3	0.8	1.29	0.17	3.0	0.5	0.088	0.003	0.003	bal.
FM60	67.2	3.2	0.08	0.07	0.2	1.5	0.004	0.014	0.003	bal.

A robotic welding system at the University of Wollongong was used to produce samples as shown in Figure 1a. The wire deposition was carried out by cold metal transfer (CMT) technology using an ABB 1400 robot with a Fronius CMT welder in flat position. Welding grade argon (99.995% purity) was used for shielding with 10 L/ min gas flow rate. Both alloy compositions (Monel K500 and FM60) have been tested in three welding conditions: 300, 400 and 500 mm/min of welding speeds and 8.3 m/min of the wire feed.

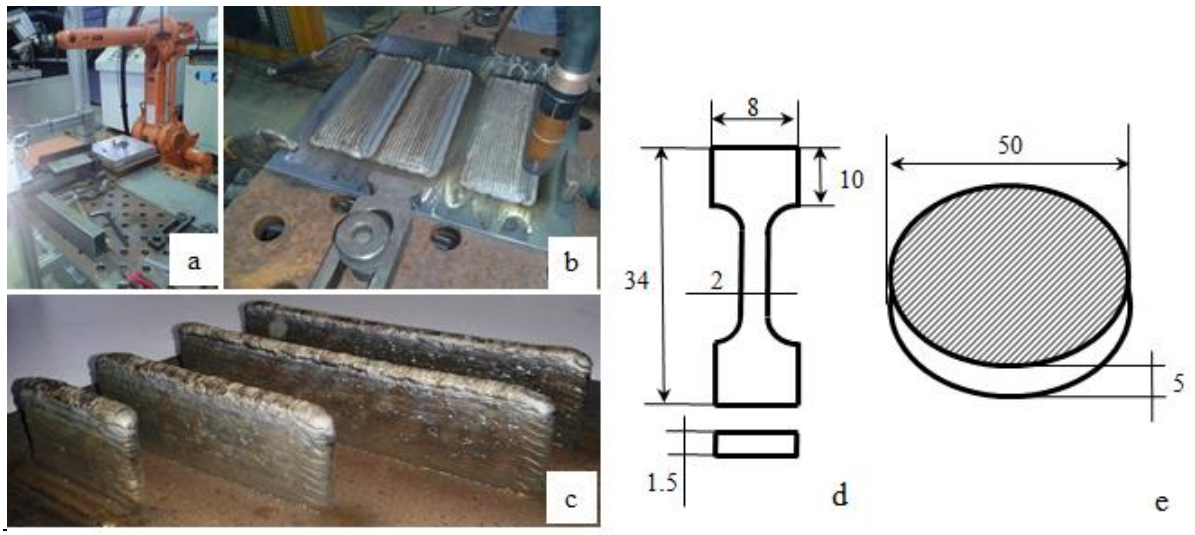

Figure 1. Illustration of the sample preparation process by WAAM: (a) experiment set-up, (b) deposition of plates, (c) deposition of multiple layered walls, (d) tensile test specimen, and (e) wear test sample geometry.

To produce samples for the wear test, multi-bead single-layer plates (55 mm wide by 180 mm long) were produced by depositing one pass of material next to the other until the required width was reached (Figure 1b). Fewer layers were required for a slower travel speed and more layers for a faster travel speed. To produce samples for the microstructure characterisation and tensile testing, single-bead multi-layer walls (40 mm high by 180 mm long) were built by depositing one layer of material on top of another until the required height was reached (Figure 1c). The number of layers varied with a welding travel speed: bigger bead was produced with slower travel speed, so that fewer layers were required to build the wall with 300 mm/min travel speed, than with 500 mm/min travel speed. All samples were cut on a horizontal band saw and wire cutting machine according to the required geometry.

Optical microscopy was carried out by using Leica M205A stereo microscope and Leica DM 600 microscope equipped with Leica Application Suite (LAS) 4.0.0 image processing software. Scanning electron microscopy was conducted using JEOL7001F FEG scanning electron microscope (SEM) operating at 10 kV. Optical microscopy and SEM were carried out on depositions cross sections. Sample preparation included mounting of samples in Polyfast resin, polishing on Struers Tegramin automatic polisher to 1 μm finish and etching with ferric chloride solution. The energy dispersive X-ray spectroscopy (EDS) semi-quantitative point analysis of precipitates and the element distribution mapping were carried out using an AZtec 2.0 Oxford SEM EDS system. For the determination of particle compositions, 40 - 60 particles were analysed from the fusion zone for each studied condition. The element distribution mapping was carried out 2-3 times from various locations for each weldment.

Tensile tests were performed on MTS Landmark servohydraulic test system, model 370.02. Flat dog-bone type samples of 10-mm gage length, 2-mm width, and 1.5-mm thickness (Figure 1, d) were cut from the deposited walls perpendicular to the direction of material deposition. For each condition, 3 samples were tested at an ambient temperature at a strain rate of 1×10^{-3} s^{-1}.

Microhardness testing was performed on all bead on plate samples on Struers DuraScan Vickers hardness tester with 0.5 kg load. The data was acquired from the base metal, heat affected zone (HAZ), remelted zone (RZ) and fusion zone (FZ). Up to ten indentations were performed in each section, with a distance of approximately ten times the length of the indent diagonals to ensure that the results were not contaminated by work hardening from previous indentations.

Wear resistance of material depositions was investigated using the pin-on-disk type of test utilised in a CETR apparatus. The wear testing was performed according to the standard ASTM G 99-95a. Discs for the wear testing were cut from the deposited plates (Figure 1, e), grinded to flat surface and polished on Struers Tegramin automatic polisher with silicon carbide polishing foil

2000 (10 micron). The stainless steel 316 ball was used as a pin. Each sample underwent 3 successive testing cycles, 750 sec of total sample-disk interaction time, track diameter 30 mm, velocity 0.758 m/c (500 rpm), total path length 600 m. One test cycle included vertical loading of the pin to 15 N load (in compression against the sample disk) and rotation of the disk for 250 sec. The wear resistance was assessed via the sample mass loss measured after each cycle (i.e. after 250, 500 and 750 sec of testing time). The sample mass was measured on fine analytical scales Nuweight AS 310.R2 with accuracy of 0.0001 gram.

3. Results and Discussion

Grain structure

Optical microscopy of 6 single weld beads deposited on Monel K500 plate was applied to analyse the shape and size variation of the bead cross sections with different welding parameters. As shown in Figure 2, with an increase in travel speed (decrease in heat input) the dilution of welds (the cross-section area of the melted base metal divided by the total area of the weld metal) decreased for both deposited materials.

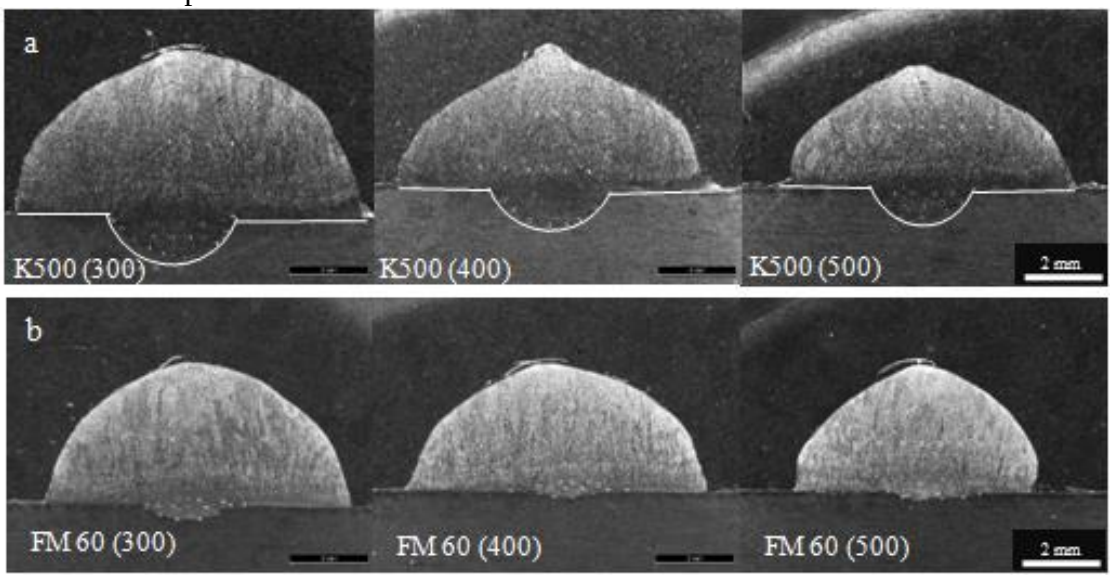

Figure 2. Optical images at low (x14) magnification taken from the cross section of single bead depositions of (a) Monel K500 and (b) FM60; the deposition speed is increasing from left to right.

The microstructure of Monel K500 base plate consisted of single phase fcc grains with average size of 25 μm. Microalloying elements particles of 200-600 nm size were evenly distributed through the volume. The mean hardness value of the plate was measured to be 170 HV. No grain growth was observed in the HAZ.

Columnar grain growth in the FZ (Figure 3a, b) and heterogeneous epitaxial grain growth in the HAZ of base metal (Figure 3c) were observed for both materials at all deposition speeds. The grain growth occurred along the heat flow direction (from the base metal towards the fusion zone). The grain size in the FZ was characterised as the secondary dendrite arm spacing, SDAS (Figure 3d and e). This was measured to be smaller in Monel K500, 4-9 μm, compared to FM60, 6-12 μm (Table 2). Probably, strong TiCN particles, present in Monel K500, effectively pinned the dendrite boundaries retarding the dendrite growth in this alloy. Capability of TiCN particles to control the grain size was previously observed in Ti-microalloyed steels [24, 25]. In Monel K500 the average SDAS slightly decreased with an increase in deposition speed (decrease in heat input), what could be a result of faster cooling, lower average temperature and less pronounced dendrite growth during deposition at a higher speed. Although in FM60 the SDAS did not vary significantly with deposition speed.

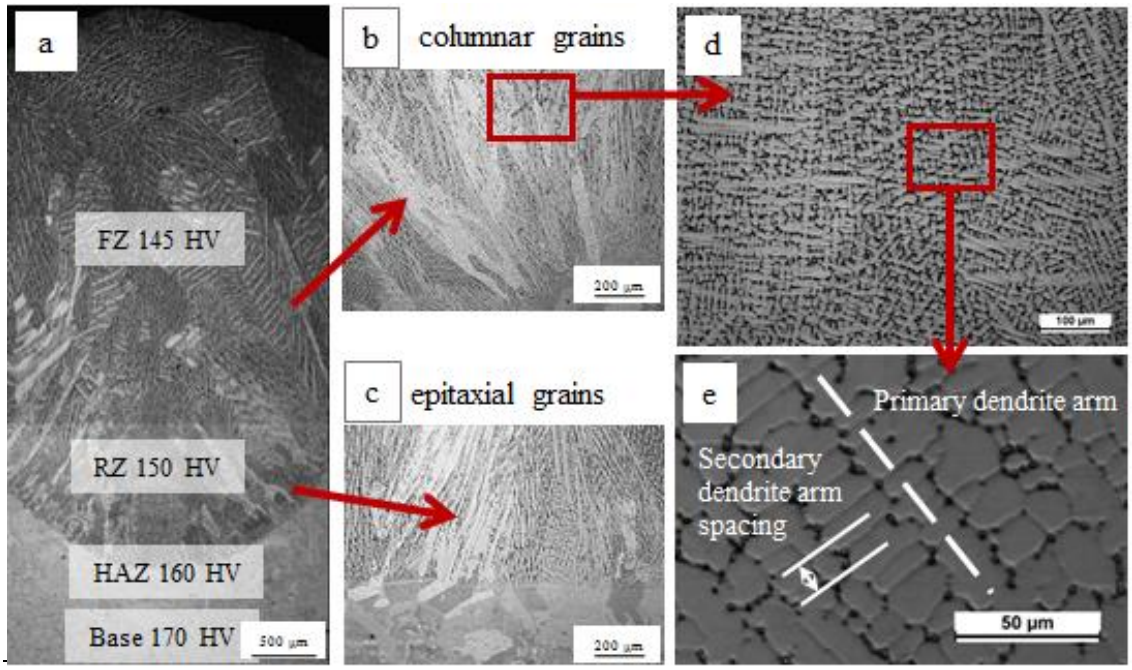

Figure 3. Optical micrographs of Monel K500: (a) welding bead cross section showing hardness variation in different welding zones, (b) columnar grains in the fusion zone, (c) epitaxial grains in the heat effected zone, (d) dendritic microstructure in the FZ and (e) a scheme of measurement of the secondary dendrite arm spacing.

Particle precipitation

Energy dispersive X-ray spectroscopy (EDS) of two alloys revealed moderate segregation of Cu in the fusion zone in all welding conditions (Figure 4a, b, d, e). This was caused primarily by the large difference in melting points of Ni (1455 °C) and Cu (1085 °C) and by the low diffusivity of Cu in Ni [26]. With a decrease in heat input the segregation decreased. No segregation was found for other alloying elements (Figure 4c, f).

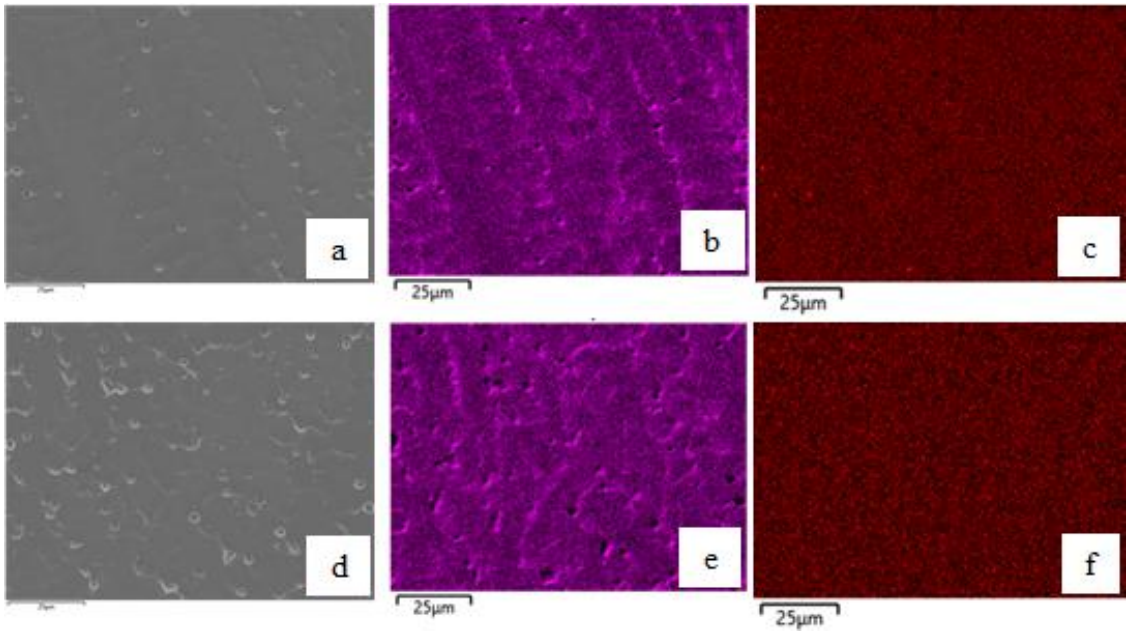

Figure 4. Representative SEM images of microstructure in (a) Monel K500 and (d) FM60, and EDS maps showing Cu segregation in (b) Monel K500 and (e) FM60 and absence of Ti segregation in (c) Monel K500 and (f) FM60.

In Monel K500 in FZ the Ti-rich particles of TiCN and TiCAlMgS type dominated (64-72% of the total amount analysed); other particles including Mn-rich ones of MnS, MnSMgO, MnMgSTiC, and MnMgSAlO type (14-18%) and Al-rich particles of AlOMgS type (11-18%) were also observed (Figure 5 a-c, Table 2). The particle sizes were in the range of 300-700 nm for 300 and 400 mm/min deposition speeds and in the range of 250-550 nm for the 500 mm/min deposition speed. The average particle size decreased with an increase in deposition speed, which can be explained by faster cooling and less time available for the particle growth. The particle number density decreased from 3.64 to 2.62 $x10^{-3}$ μm^{-2} with an increase in deposition speed from 300 to 500 mm/min, which is consistent with the decrease in average particle size.

In FM60 in FZ the majority of particles were Mn-rich of MnSMgO and MnSAlMgCaO type (66 to 80% of the total amount analysed); Ti-rich ones of TiAlMgO and TiSAlMgO type (18-30%) and Al-rich particles of AlMgO type (2-7%) were also present (Figure 5 d-f, Table 2). It is worth to note a much lower fraction of Ti-rich particles in FM60, compared to Monel K500, although the Ti content in FM60 composition is higher. This could result from a lower carbon and nitrogen contents in FM60, and a possible increase in solubility of Ti in FM60 due to increased Mn content. In Ti-microalloyed steels the rate of Ti particle precipitation has been shown to decrease with an increase in Mn content [27, 28]. The particle sizes were in the range of 200-800 nm for all deposition speeds. The average particle size showed a maximum at the speed of 400 mm/min, although the particle size variation with deposition speed was within the measurement error. The particle number density in FM60 decreased from 11.4 to 4.7 $x10^{-3}$ μm^{-2} with an increase in deposition speed from 300 to 500 mm/min, which is consistent with the similar trend in Monel K500. The average particle size was slightly larger in Monel K500 than in FM60, because the temperature of TiCN precipitation is usually higher (1000-1500 °C [29]) than that of MnS precipitation (800-1000 °C [30]). Thus, TiCN particles have more time for growth.

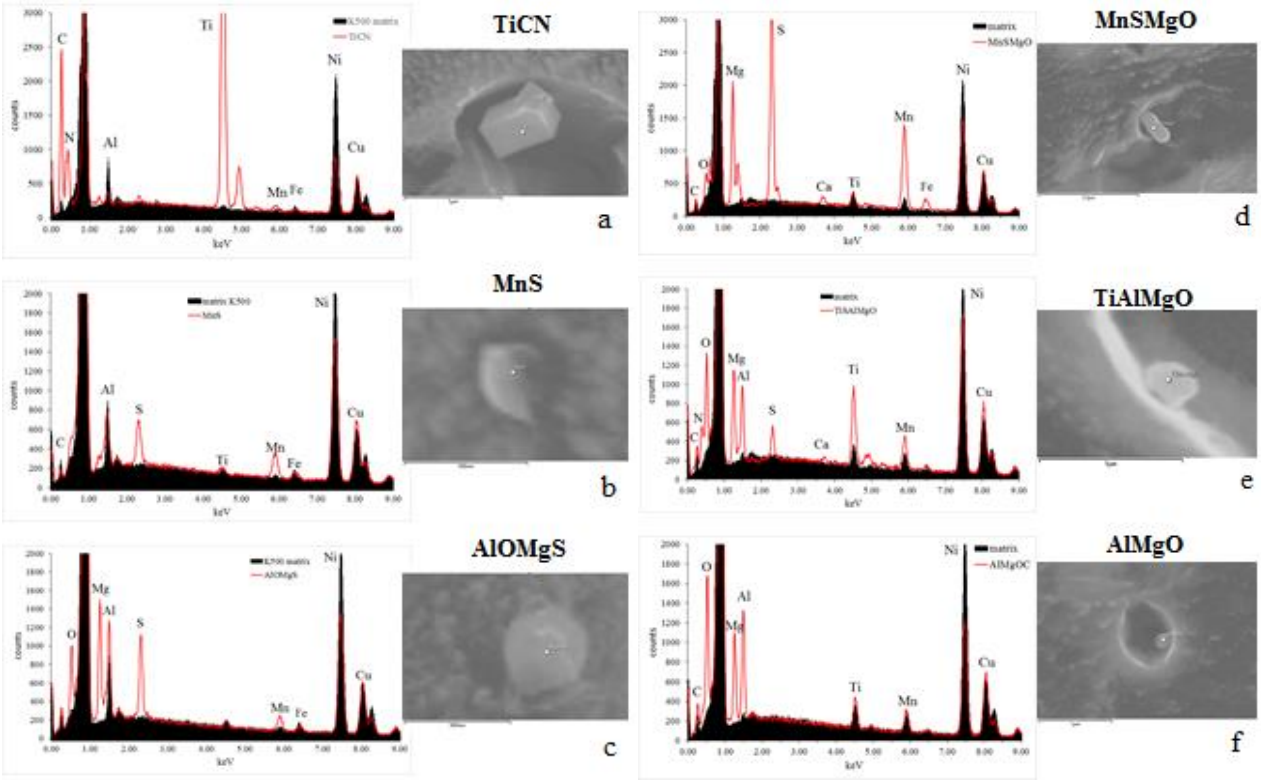

Figure 5. EDS spectra showing chemical composition of particles in deposited (a-c) Monel K500 and (d-f) FM60; the matrix spectrum is shown in black, the particle spectrum is shown in red.

Table 2. Microstructural parameters and mechanical properties of the studied alloys.

Parameter		Monel K500			FM60		
		300	400	500	300	400	500
SDAS, μm		6-9	5-9	4-8	6-10	6-12	6-10
Particles	size, nm	437±150	448±140	331±160	311±170	392±150	388±160
	ND* $x10^{-3}$ μm^{-2}	3.64	3.06	2.62	11.39	7.24	4.71
	Chemistry, %	72Ti-rich 17Mn-rich 11Al-rich	69Ti-rich 14Mn-rich 17Al-rich	64Ti-rich 18Mn-rich 18Al-rich	67Mn-rich 26Ti-rich 7Al-rich	66Mn-rich 30Ti-rich 4Al-rich	80Mn-rich 18Ti-rich 2Al-rich
Hardness in FZ/RZ/HAZ		141/145/ 156	144/146/ 159	145/152/ 163	134/135/ 141	133/135/ 139	136/137/ 142
YS, MPa		170±5	165±10	160±5	146±14	160±12	150±5
UTS, MPa		430±15	410±10	408±15	356±10	363±20	360±5
Elongation, %		47±2	51±3	50	48±3	47±1	48±2
MPa·%		14100	14662	14200	12048	12290	12240
Wear mass loss, g		0.0560	0.0420	0.0460	0.0622	0.0574	0.0628

ND* - number density of particles

Mechanical properties and wear resistance

The microhardness (HV), yield stress (YS) and ultimate tensile strength (UTS) in Monel K500 plates obtained in this work using WAAM were in the range of 141-163 HV, 160-170 MPa and 408-430 MPa, respectively. This is about 1.7, 2.4 and 1.6 times lower than the values expected for a cast microstructure, 277 HV, 415 MPa and 690 MPa, respectively [31]. In accordance with lower strength, the elongation to failure (El) 47-51 % was 5 times higher than this for a cast microstructure, 10 %. On the contrary, hardness 133-142 HV, YS = 146-160 MPa and UTS = 356-363 MPa in FM60 were only 5.5, 6 and 24 % lower than the corresponding values in cast Monel 400 with composition similar to FM60, 150 HV, 170 MPa and 450 MPa, respectively. And the elongation to failure, 48 % in FM60, was about 2 times higher compared to the cast Monel 400, 25 % [31]. The significant variation in properties of Monel K500 could be explained by the variation in cooling rates between WAAM and casting: very fast cooling rates (short cooling time) inherent for WAAM prevent particle precipitation required for enhanced strength of Monel K500. However, for FM60 the same variation in cooling rates is not so critical for the mechanical properties variation, because the FM60 and Monel 400 are not designed for age-hardening (the precipitation strengthening mechanism is weak). Analysis of the stress-strain curves (Figure 6 a-c) has shown that Monel K500 exhibits slightly higher YS, UTS and elongation to failure than FM60, which was expected due to the variation in alloy composition, in particular a higher C content (Table 2). Although the particle number density measured using SEM imaging was higher in FM60, a higher C content in Monel K500 could result in more pronounced particle precipitation in the <15 nm size range. This would explain higher strength and ductility in Monel K500. To support this a more detailed characterisation of particles with transmission electron microscopy is required. For the tested deposition speed range, no significant variation in tensile properties with speed was observed. Toughness, evaluated as a product of 0.5(YS·UTS) and El [32], was higher in Monel K500 than in FM60. This corresponds to the higher strength and ductility of Monel K500. For both alloys the maximum average toughness was observed for the medium deposition speed of 400 mm/min.

The average microhardness of Monel K500 depositions decreased from 170 HV for the base metal to 160 HV for HAZ, to 150 HV for the remelted zone and to 145 HV for the fusion zone (Figure 6 d-f). The average microhardness of FM60 depositions decreased from 170 HV for the base metal to 140 HV for HAZ, to 135 HV for the remelted and fusion zones. The decreased microhardness in HAZ, compared to the base metal, can be related to stress relief and dislocation

annihilation following heating in this area. Remelted and fusion zones exhibited typical cast microstructure the hardness of which is obviously lower than that of base metal with deformed microstructure. The microhardness in different zones of the weld cross section did not vary significantly with the deposition speed for both alloys (Table 2). However, the hardness of Monel K500 was definitely higher than that of FM60 for all deposition speeds, which corresponds to the smaller SDAS and precipitation of hard TiCN particles in Monel K500.

The wear resistance of Monel K500 depositions was higher (mass loss lower) than that of FM60 depositions for all three speeds (Figure 6g-e). This corresponds to the higher hardness and toughness of Monel K500, related to its smaller SDAS and precipitation of hard TiCN particles. For both alloys the highest toughness at 400 mm/min deposition speed corresponded to the highest wear resistance (lowest mass loss during the wear testing) for this speed. An increase in wear resistance with an increase in hardness was previously observed in medium carbon steels [33, 34]. In particular, wear resistance increased with precipitation of hard Nb- and Cr-rich carbides [35, 36]. On another hand, increased toughness, or rather a proper balance between hardness and toughness, was suggested to be the major reason for increased wear resistance [37, 38].

On the next stage of our research we are going to modify the precipitate distributions with age-hardening heat treatment and further improve the mechanical properties of WAAM-deposited Ni-Cu alloys. In addition to the Ti-rich particles, Ni-rich gamma prime particles may be expected to affect the microstructure-properties relationship in the studied alloys. However, due to their small size, <15 nm, they cannot be observed in SEM. Therefore, an in-depth study of precipitates will be conducted using transmission electron microscopy.

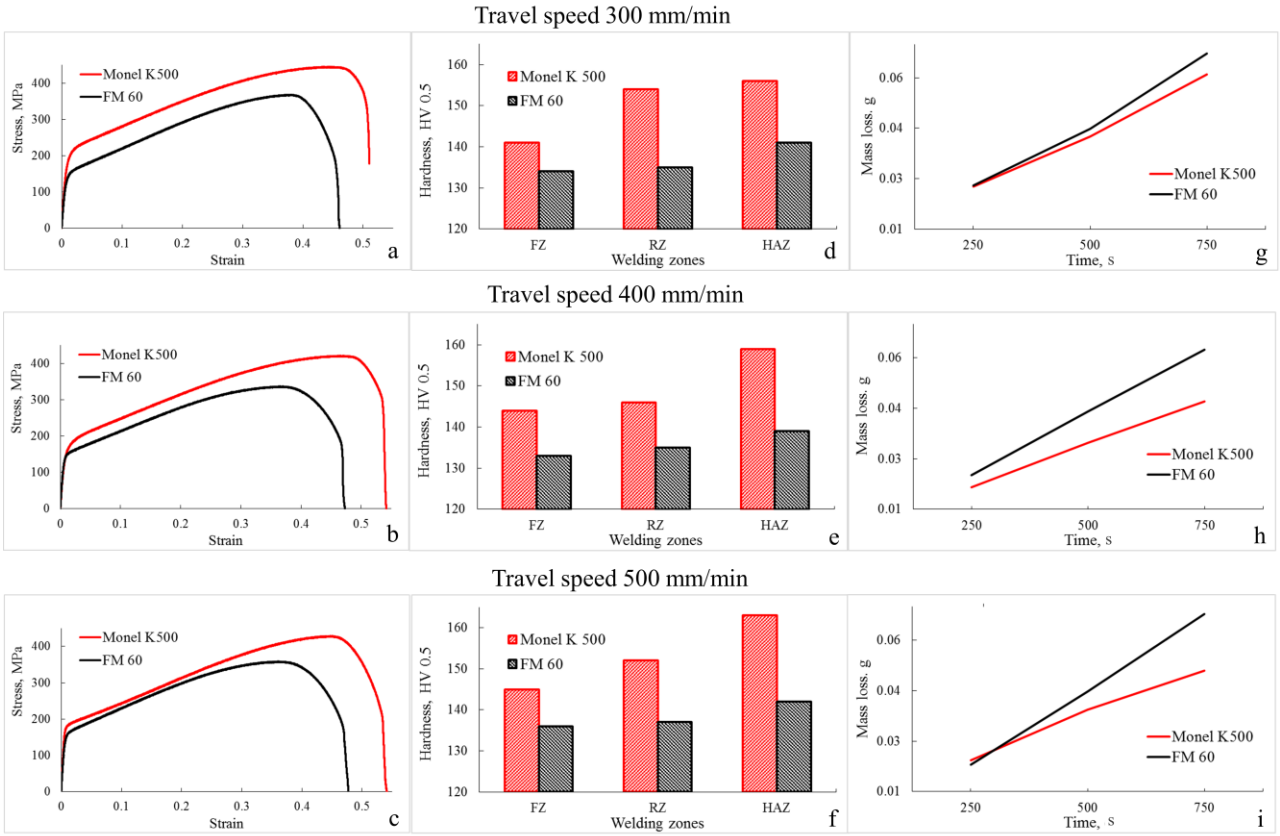

Figure 6. Mechanical properties of wire deposited Monel K500 (red) and FM60 (black) for the three studied deposition speeds: (a-c) tensile stress-strain curves; (d-f) hardness in different zones of the weld cross section; and (g-i) wear resistance (mass loss).

Conclusions

Investigation of the microstructure and mechanical properties of WAAM-produced Ni-Cu alloys resulted in the following conclusions:

1. In Monel K500 the secondary dendrite arm spacing was smaller than in FM60, which corresponded to a higher number density of TiCN precipitates in Monel K500.
2. Moderate Cu segregation in depositions was observed in both alloys. This could result from a variation in the Ni and Cu solidification temperatures irrespective of other elements concentrations.
3. The majority of precipitates were Ti-rich particles in Monel K500 and Mn-rich ones in FM60, although the Ti content is higher in FM60. This could result from the lower carbon and nitrogen contents in FM60 and a possible increase in Ti solubility in FM60 due to an increased Mn content in it. With an increase in deposition speed the particles number densities decreased in both alloys, which can be explained by a faster cooling rate (less time available for precipitation) for a faster deposition speed.
4. Hardness, strength, ductility, toughness and wear resistance were higher in Monel K500, compared to FM60. This mainly resulted from the precipitation of Ti-rich particles in Monel K500. For both alloys the highest wear resistance corresponded to the highest toughness observed at the medium deposition speed of 400 mm/min.

Acknowledgement

This project was financially supported by the Defence Materials Technology Centre (DMTC), which was established under the initiative of Australian Government's Defence Future Capability Technology Centre (DFCTC). Olexandra Marenych is thankful for a scholarship sponsored by DMTC. The WAAM was carried out in the UOW Welding and Industrial Automation Research Centre. Assistance of Dr. Chen Shen with tensile tests is greatly appreciated. The JEOL JSM-7001F FEG-SEM used in this work for microstructure characterisation was funded by the Australian Research Council grant LE0882613.

References

[1] T.H. Bassford, J. Hosier, Nickel and its Alloys, in: M. Kutz (Ed.), Handbook of materials selection, Wiley, New York, 2002.

[2] J.C. Lippold, J.N. DuPont, S.D. Kiser, Welding metallurgy and weldability of Nickel-base alloys, Wiley, New York, 2009.

[3] High-performance alloys for resistance to aqueous corrosion, Publication number SMC-026, Special Metals Corporation, 2000, https://www.scribd.com/document/55871734/Nickel-Base, (accessed 12 December 2017).

[4] R.W. Kozar, A. Suzuki, W.W. Milligan, J.J. Schirra, M.F. Savage, T.M. Pollock, Strengthening mechanisms in polycrystalline multimodal nickel-base alloys, Metall. Mater. Trans. A, 40 (2009), pp. 1588 – 1603.

[5] J.R. Davis, Nickel, Cobalt, and their Alloys, ASM International, Materials Park, OH, USA, 2000.

[6] Product handbook of high performance alloys, Publication number SMC-035, Special Metals Corporation, 2008, https://www.scribd.com/document/320420951/Special-Metals-Product-Handbook, (accessed 12 December 2017).

[7] E.W. Ross, C.T. Sims. Nickel-base alloys, in: C.T. Sims, N.S. Stoloff, W.C. Hagel (Eds.) Superalloys II: High Temperature Materials for Aerospace and Industrial Power, ASM International, Materials Park, OH, 1987, pp. 97-133.

[8] Review of the wear and galling characteristics of stainless steels, American Iron and Steel Institute, 1978, https://www.nickelinstitute.org (accessed 12 December 2017).

[9] D. D. Gu, W. Meiners, K. Wissenbach, R. Poprawe, Laser additive manufacturing of metallic components: materials, processes and mechanisms, Int. Mater. Rev. 57 (2012), pp. 133-164.

[10] R. Acheson, Automatic welding apparatus for weld build-up and method of achieving weld build-up, US patent no. 4 952 769 1990.

[11] D. Ding, Z. Pan, D. Cuiuri, H. Li, Wire-feed additive manufacturing of metal components: technologies, developments and future interests, Int. J. Adv. Manuf. Tech., 81 (2015), pp. 465-481.

[12] D. Ding, Z. Pan, D. Cuirui, H. Li, A practical path planning methodology for additive manufacturing of thin-walled structures. Robot. Com-Int. Manuf., 34 (2015), pp. 8–19.

[13] Y. Ma, D. Cuiuri, C. Shen, H. Li, Z. Pan, The effect of location on the microstructure and mechanical properties on in-situ alloying and additive layer manufacturing of titanium aluminides using gas tungsten arc welding, Mater. Sci. Eng. A, 631 (2015), pp. 230–240.

[14] F. Martina, J. Mehnen, S.W. Williams, P.A. Colegrove, F. Wang, Investigation of the benefits of plasma deposition for the additive layer manufacture of Ti–6Al–4V, J. Mater. Process. Technol., 212 (2012), pp. 1377–1386.

[15] S. W. Williams, F. Martina, A. C. Addison, J. Ding, G. Pardal, P. Colegrove, Wire + Arc Additive Manufacturing, Mater. Sci.Tech., 32 (2016), pp. 641-647.

[16] B. Wu, D. Ding, Z. Pan, D. Cuiuri, H. Li, J. Han, Z. Fei, Effects of heat accumulation on the arc characteristics and metal transfer behavior in Wire Arc Additive Manufacturing of Ti6Al4V, J. Mater. Process. Tech., 250 (2017), pp. 304-312.

[17] F. Wang, S. Williams, M. Rush, Morphology investigation on direct current pulsed gas tungsten arc welded additive layer manufactured Ti6Al4V alloy, Int. J. Adv. Manuf. Tech., 57 (2011), pp. 597–603.

[18] C.V. Haden, G. Zeng, F.M. Carter III, C. Ruhl, B.A. Krick, D.G. Harlow, Wire and arc additive manufactured steel: tensile and wear properties. Addit. Manuf., 16 (2017), pp. 115-123.

[19] C. Shen, Z. Pan, D. Cuiuri, D. Ding, H. Li, Influences of deposition current and interpass temperature to the Fe3Al-based iron aluminide fabricated using wire-arc additive manufacturing process, Int. J. Adv. Manuf. Technol., 88 (2017), pp. 2009-2018.

[20] B. Cong, J. Ding, S. Williams, Effect of arc mode in cold metal transfer process on porosity of additively manufactured Al-6.3%Cu alloy, Int. J. Adv. Manuf. Technol., 76 (2015), pp. 1593-1606.

[21] D. Ding, Z. Pan, S. van Duin, H. Li, C. Shen, Fabricating superior NiAl Bronze components through wire arc additive manufacturing, Materials 9 (2016), paper 652.

[22] F.J. Xu, Y.H. Lv, B.S. Xu, Y.X. Liu, F.Y. Shu, P.He, Effect of deposition strategy on the microstructure and mechanical properties of Inconel 625 superalloy fabricated by pulsed plasma arc deposition, Mater. Design 45 (2013), pp. 446-455.

[23] B. Baufeld, Mechanical properties of Inconel 718 parts manufactured by shaped metal deposition (SMD), J. Mater. Eng. Perform., 21 (2012), pp.1416-1421.

[24] J. Strid, K.E. Easterling. On the chemistry and stability of complex carbides and nitrides in microalloyed steels, Acta Metall., 33 (1985), pp. 2057-2074.

[25] R.D.K. Misra, H. Nathani, J.E. Hartmann, F. Siciliano, Microstructural evolution in a new 770MPa hot rolled Nb-Ti microallyed steel, Mater. Sci. Eng. A, 394 (2005), pp. 339-352.

[26] R.W. Heckel, J.H. Rickets, J. Busgwald, Measurement of the degree of segregation in Monel 400 weld metal by X-ray line broadening, Weld. J., 34 (1965), pp. 332-336.

[27] M. G. Akben, T. Chandra, P. Plassiard, J.J. Jonas, Dynamic precipitation and solute hardening in a titanium microalloyed steel containing three levels of manganese, Acta Metall., 32(4) (1984), pp. 591-601.

[28] Z. Wang, X. Sun, Z. Yang, Q. Yong, C. Zhang, Z. Li, Y. Weng, Effect of Mn concentration on the kinetics of strain induced precipitation in Ti microalloyed steels, Mater. Sci. Eng. A, 561 (2013), pp. 212-219.

[29] R. Soto, W. Saikaly, X. Bano, C. Issartel, G. Rigaut, A. Charai, Statistical and theoretical analysis of precipitates in dual-phase steels microalloyed with titanium and their effect on mechanical properties, Acta Metall., 47(12) (1999), pp. 3475-3481.

[30] Y. Chen, Y. Wang, A. Zhao, Precipitation of AlN and MnS in low carbon aluminium killed steel, J. Iron Steel Res. Int., 19(4) (2012), pp. 51-56.

[31] https://www.metaltek.com (accessed 15 December 2017).

[32] Z.P. Xiong, A.G. Kostryzhev, A.A. Saleh, L. Chen, E.V. Pereloma. Microstructures and mechanical properties of TRIP steel produced by strip casting simulated in the laboratory, Mater. Sci. Eng. A, 664(2016), pp. 26-42.

[33] K. Luo, B. Bai, Microstructure, mechanical properties and high stress abrasive wear behaviour of air-cooled MnCrB cast steels, Mater. Design 31 (2010), pp. 2510-2516.

[34] W. Wang, R. Song, S. Peng, Z. Pei, Multiphase steel with improved impact-abrasive wear resistance in comparison with conventional Hadfield steel, Mater. Design 105 (2016), pp. 96-105.

[35] S. Huth, N. Krasokha, W. Theisen, Development of wear and corrosion resistant cold-work tool steels produced by diffusion alloying, Wear 267 (2009), pp. 449-457.

[36] M. Lindroos, K. Valtonen, A. Kemppainen, A. Laukkanen, K. Holmberg, V.-T. Kuokkala, Wear behavior and work hardening of high strength steels in high stress abrasion, Wear 322-323 (2015), pp. 32-40.

[37] H. Fu, Q. Xiao, H. Fu, Heat treatment of multi-element low alloy wear-resistant steel, Mater. Sci. Eng. A, 396 (2005), pp. 206-212.

[38] G. Bregliozzi, A.Di Schino, J.M. Kenny, H. Haefke, The influence of atmospheric humidity and grain size on the friction and wear of AISI 304 austenitic stainless steel, Mater. Lett. 75 (2003), pp. 4505-4508.